Clays and Clay Minerals, Vol. 54, No. 1, 87–100, 2006.

WEATHERING SEQUENCES OF ROCK-FORMING MINERALS IN A SERPENTINITE: INFLUENCE OF MICROSYSTEMS ON CLAY MINERALOGY

J. Caillaud[1,*], D. Proust[2] and D. Righi[2]

[1] FRE 2816 CNRS, ELICO, Université du Littoral Côte d'Opale, MREN, 32 Avenue Foch, 62930 Wimereux, France
[2] UMR 6532 CNRS, HydrASA, Faculté des Sciences, 40 av. du recteur Pineau, 86022 Poitiers cedex, France

Abstract—Under closed geochemical conditions, the weathering of a serpentinite rock composed of serpentine (70−85%) and magnesian chlorite (10−15%) associated with magnetite and chromite leads to the complete replacement of serpentine and chlorite by 2:1 layer silicates and produces new Fe oxides. The serpentine minerals crystallize under different habits issued from the serpentinization processes: mesh and hourglass pseudomorphic textures were formed from olivine, and thin-bladed pseudomorphic textures from pyroxene and amphibole crystals. Serpentine veins crosscut the whole rock with locally non-pseudomorphic interpenetrating and interlocking serpentines.

Specific weathering microsystem habits with specific clay mineral crystallizations originate from these different habits: a poorly aluminous saponite in thin-bladed textures, two Fe-rich montmorillonites in mesh and hourglass (MH) textures, and in veins (V) which differentiate on Al, Mg and Fe contents. Magnesian chlorites, isolated from serpentine by hand-picking under a stereomicroscope, are found to weather to trioctahedral vermiculite. Magnetite and chromite extracted from the bulk samples are replaced by newly formed Fe oxides, maghemite, goethite and hematite, which give way to specific Fe accumulation habits in the regolith zone of the weathering profile.

Key Words—Iron, Regolith, Serpentinite, Texture, Weathering.

INTRODUCTION

Many ultramafic rocks are hydrated to form partially or completely serpentinized rocks. Serpentinites are Mg-rich rocks resulting from metamorphic alteration of dunite, peridotite or pyroxenite and are composed essentially of serpentine minerals. Serpentine is the family name for three major minerals: lizardite (planar structure), chrysotile (cylindrical rolls) and antigorite (alternating wave structure). Serpentinization processes in naturally occurring ultramafic rocks have been widely studied. Studies have notably been concerned with: (1) the influence of the parent rock mineralogy (dunite, peridotite or pyroxenite) on the alteration minerals during the serpentinization processes (Hostetler *et al.*, 1966; Wicks, 1969; Coleman and Keith, 1971); (2) the temperature-pressure regime of hydration (Johannes, 1968; Chernosky, 1973); (3) the influence of fluid origin and composition on hydration (Johannes and Metz, 1968; Barnes and O'Neil, 1969; Barnes *et al.*, 1972; Moody, 1974; Wenner and Taylor, 1974); and (4) the mineralogical assemblages produced during serpentinization (Wicks, 1969; Coleman, 1971; Wenner and Taylor, 1971). Wicks and Whittaker (1977) improved the identification of the serpentine textures by using a microbeam X-ray diffraction camera and demonstrated that they could be divided into three types: pseudomorphic textures formed essentially from olivine, pyroxene and amphibole, non-pseudomorphic textures, and textures formed from serpentine veins. These serpentine textures are expected to induce different alteration systems producing specific clay minerals.

Numerous studies of serpentinite weathering under temperate conditions deal specifically with bulk mineralogical and chemical properties of serpentinite-derived pedons (Rabenhorst *et al.*, 1982; Alexander *et al.*, 1989; Graham *et al.*, 1990; Bulmer and Lavkulich, 1994). These studies demonstrate the large variety of clay phases produced by serpentine weathering processes and the influence of topographic position and moisture conditions upon the development of the weathering profiles (Coombe *et al.*, 1956; Wildman *et al.*, 1968; Berre *et al.*, 1974; Ducloux *et al.*, 1976; Istok and Harward, 1982; Bonifacio *et al.*, 1996; Lee *et al.*, 2001, 2003). More detailed studies of felsic rocks and their weathering products were carried out at the scale of the weathering minerals introducing the concept of 'microsystems' (Meunier, 1977; Ildefonse, 1978; Fontanaud, 1982; Proust, 1983; Hochella and Banfield, 1996). These studies demonstrated that clay minerals forming in weathering profiles could vary according to the site in which reaction occurs. Clay minerals appear to be mineralogically and chemically different according to the crystallization microsite that includes grain fractures in rock-forming minerals, microcracks and larger pores.

The literature dealing with serpentinite weathering at the microsystem scale is relatively sparse and consequently, precise knowledge of the processes involved

* E-mail address of corresponding author:
jacinthe@mren2.univ-littoral.fr
DOI: 10.1346/CCMN.2006.0540111

should be improved at this scale. This study was thus focused on the different rock-forming minerals in a serpentinite in order to characterize weathering products, taking into account the reaction location (microsites). The study of bulk clay minerals formed by serpentinite weathering (Caillaud *et al.*, 2004) could then be compared with the individual rock-forming mineral contribution.

MATERIALS AND METHODS

Materials

The studied materials were located 30 km south of Limoges, near the village of La Roche l'Abeille (Limousin, France) and were extracted from the weathering profile described by Caillaud *et al.* (2004). The samples were collected from three alteration zones: (1) unweathered rock, (2) the saprock, where coherent rock structure is still preserved, and (3) the regolith, in which the texture of the original rock was lost and replaced by a mixture of clay associated with oxyhydroxides and relics of rock-forming minerals.

Minerals from the serpentinite (serpentine, chlorite and magnetite) were specifically studied in this work in order to specify their own weathering products in the three different alteration zones.

Methods

Weathering products from serpentinite were studied in their crystallization sites as observed by optical microscopy of thin-sections. They were identified using their chemical composition from electron microprobe analyses (EMPA) and calculation of their structural formulae. Separation of serpentine from chlorite was tested using heavy liquids (sodium polytungstate) and magnetic separation. These methods were not efficient because the two minerals have very similar density and magnetic properties. Serpentine minerals extracted by hand-picking and checked for purity by powder X-ray diffraction (XRD) showed that small chlorite crystals were always present and intimately associated. Thus, pure serpentine minerals could not be separated. Pure chlorite was successfully separated from serpentines by hand-picking 100−250 μm sized crystals under the stereomicroscope. Their weathering products were characterized using XRD, EMPA and scanning electron microscopy (SEM).

Magnetite and chromite were extracted from bulk samples using a hand magnet. Magnetic fractions containing magnetites, chromites and secondary oxyhydroxides were studied using XRD and *in situ* EMPA in thin-sections.

The petrographic data were recorded from thin-sections using optical microscopy (Olympus BH2) under plane- and crossed-polarized light, and SEM (Jeol JSM6400) equipped with an energy dispersive spectrometer (EDS) for chemical analysis. The SEM observations were made in the secondary electron mode for morphological investigations and the backscattered mode for chemical mappings.

Chemical analyses were obtained from thin-sections using a CAMECA SX 50 electron microprobe (Camparis, Université Pierre et Marie Curie, Paris) with wavelength-dispersive spectrometers (WDS). The major elements analyzed were Na, Mg, Al, Si, K, Ca, Ti, Cr, Ni, Mn and Fe. The microprobe was calibrated using synthetic and natural oxides. The analytical conditions were as follows: current intensity − 4 nA; accelerating voltage − 15 kV; spot size − 1 μm; counting time 10 s per element. Corrections were made with a ZAF program. The relative error for the analyzed elements is <1.5%.

The XRD studies were performed using a Siemens Kristalloflex 810 diffractometer (40 kV, 30 mA) with a Ni-filtered Cu$K\alpha_{1,2}$ radiation (λ = 1.5418 Å). Chlorite samples were examined as parallel-oriented clay mineral aggregates. The XRD patterns were obtained using a DACO-MP multichannel recorder associated with a microcomputer using the Diffract-AT software (SOCABIM). The XRD studies on the magnetic fraction were carried out using a Philips P.W. 1729 diffractometer (40 kV, 40 mA) and Fe-filtered Co$K\alpha_{1,2}$ radiation (λ = 1.7902 Å) because this fraction is composed of Fe-rich particles. Samples were examined as randomly oriented powders.

For chlorite samples, pre-treatment of the specimens included Ca saturation and solvation with ethylene glycol. The smectite mean layer charge was calculated according to the method of Olis *et al.* (1990), who correlated the mean layer charge of smectites with their d_{001} spacings after expansion with single, long-chain alkylammonium ions (nC = 12).

RESULTS

Rock-forming minerals

Serpentine minerals. Under the petrographic microscope (crossed polarizers), the serpentine minerals show different habits (Figure 1): (1) mesh and hourglass pseudomorphic textures were derived from olivine, and thin-bladed textures were formed in pyroxene and amphibole crystals; (2) serpentine fiber rims, which line mesh and hourglass textures; and (3) serpentine veins, which crosscut the whole rock. Brucite that may form during serpentinization processes (Johannes, 1968) was not identified in the thin-sections because, if present, it is probably fine-grained and intergrown with lizardite and/or chrysotile.

The XRD pattern of the unweathered rock powder shows the major reflections at 7.30, 4.56, 3.65, 2.65 and 2.49 Å of the serpentine minerals, lizardite and chrysotile (Figure 2). No antigorite peak was observed. Brucite would be identified by its characteristic XRD reflection at 4.77 Å and 2.37 Å in XRD if present in the rock in

https://doi.org/10.1346/CCMN.2006.0540111 Published online by Cambridge University Press

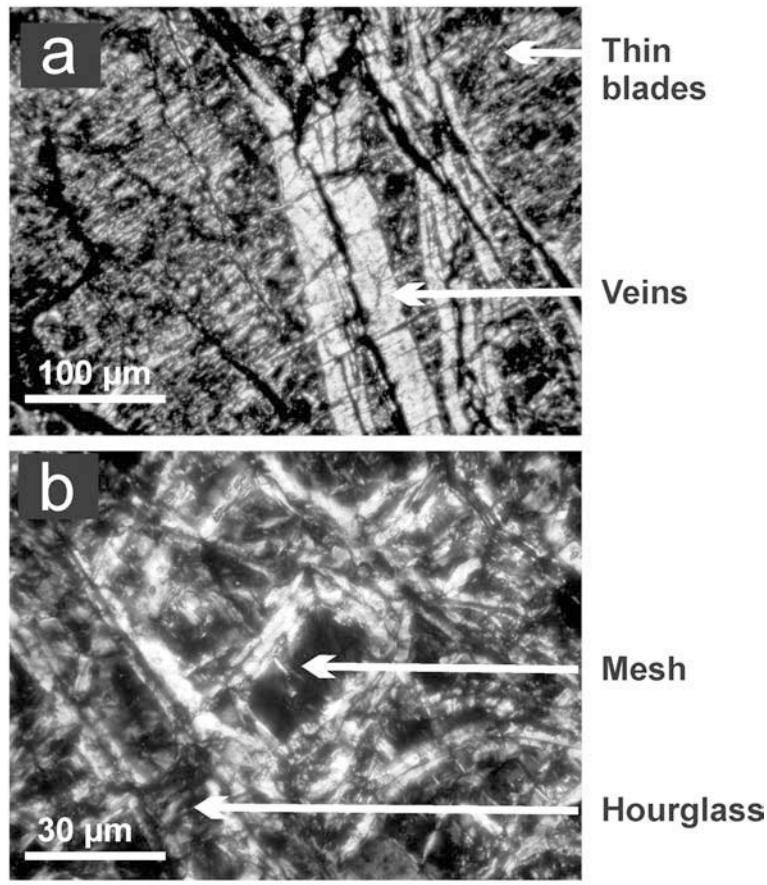

Figure 1. Optical micrographs, under crossed nicols, of serpentine habits: (a) thin-bladed serpentine texture crosscut by chysotile vein; (b) mesh and hourglass serpentine texture.

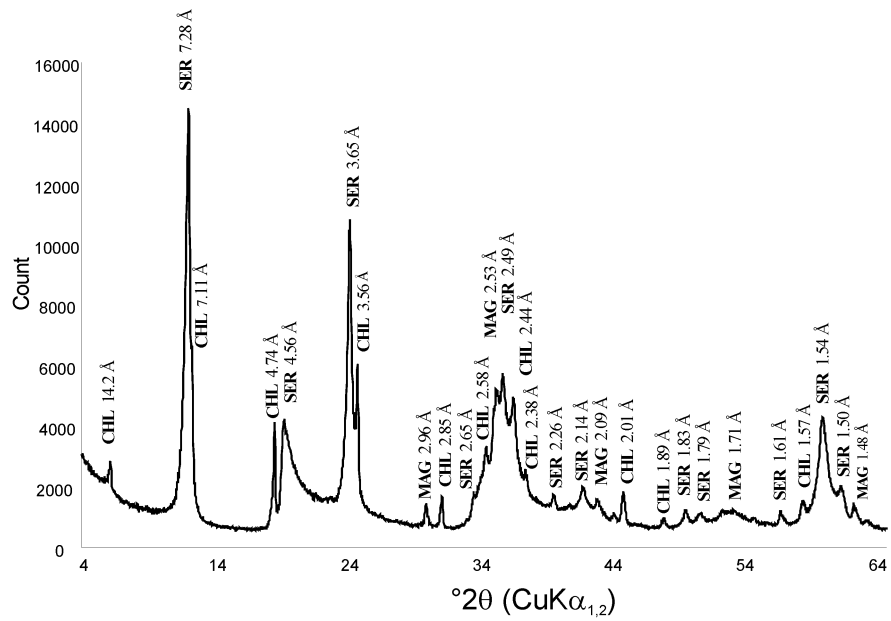

Figure 2. XRD powder pattern of the unweathered rock sample. CHL – chlorite; SER – serpentine; MAG – magnetite.

https://doi.org/10.1346/CCMN.2006.0540111 Published online by Cambridge University Press

amounts >2% (Hostetler *et al*., 1966). In the present case, superposition of peaks from chlorite and lizardite does not allow identification of brucite.

A structural classification of 12 different trioctahedral 1:1 polytypes of lizardite minerals was proposed by Bailey (1969). The 12 polytypes are distributed into four groups (A-B-C-D). According to the XRD pattern from the rock powder, the 2.49 Å reflection is intense, as in the B, C and D groups. The most intense reflection at 2.326 Å of group B and the 1.945 Å peak of groups B and D are absent on the XRD pattern of the whole rock. In addition, the absence of a 2.387 Å reflection precludes the occurrence of group A. Thus, the lizardite minerals belong to group C (1T-2T-3R).

Under crossed nicols, the chrysotile mineral presents the straight extinction of orthochrysotile specimen ($2Or_{c1}$), according to the notation for cylindrical structures (Wicks and Whittaker, 1975).

Results of the EMPA analysis of serpentine minerals in the unweathered rock are given in Table 1. Chemical compositions of serpentine in the different habits show small but significant variations: (1) mesh or hourglass serpentine has relatively high Fe and Ni contents (4.08% and 0.48% oxides, respectively); (2) thin-bladed serpentine has a low SiO_2 content (38.15%) and a relatively large amount of Al_2O_3 (2.82%) and chromium (0.77% oxides), but these last two high values may be due to the presence in the analyzed spot of small interpenetrating chlorites; (3) serpentine in veins has small Al_2O_3 contents (0.09% oxides) and relatively large MgO values (37.28% oxides). These chemical variations are in agreement with the data of Whittaker and Wicks (1970) and Dungan (1974) for serpentine compositions.

Chlorite. Petrographic observation characterizes chlorite as a well crystallized mineral, colorless under plane-polarized light and olive green under crossed polarizers. Crystals are between 10 and 350 μm wide and are intimately associated with serpentine and magnetite.

The XRD pattern of the unweathered rock shows the rational series of chlorite basal spacings at 14.20, 7.10, 4.74, 3.56 and 2.85 Å, which do not change after ethylene glycol solvation (Figure 2).

The results of EMPA analyses of chlorite in the unweathered rock are given in Table 2. Chlorite appears to be the main Al-bearing rock-forming mineral in the rock (14% oxide) with homogeneous composition including: (1) a large amount of MgO; (2) very small FeO contents; and (3) relatively large Cr_2O_3 values (~2% oxide). These chemical analyses were used to calculate a mean structural formula on the basis of 14 oxygen atoms (Table 2); the calculation of octahedral occupancy close to 6 demonstrates that the chlorite is trioctahedral. A Mg octahedral cation indicates a clinochlore composition with a tetrahedral charge between 0.8 and 0.9 per half unit-cell. The structural formulae plotted in a $Si-R^2-R^3$ ternary diagram show the homogeneous composition of the rock chlorite (Figure 3).

Magnetite and chromite. Petrographic observations show that thin magnetite veinlets (0.5 mm) surrounding the mesh or hourglass textural units are included in serpentine fiber rims. Thicker (mm) magnetite and chromite veins often interlock into chlorite, and sometimes into serpentine.

The XRD pattern of unweathered rock shows intense reflections at 2.53 and 2.96 Å which are typical of magnetite and chromite (Figure 2).

The EMPA results are given in Table 3. Magnetites are characterized by very large Fe contents, between 80 and 90% oxides, and chromites by Cr and Fe values close to 42% and 45% oxides, respectively. The high Fe and low Al contents in chromite composition may result

Table 1. EMPA (*n* analyses) of serpentine minerals in the unweathered rock (wt.% oxides).

	Mesh or hourglass serpentine		Thin bladed serpentine		Serpentine veins and fiber rims	
	Mean (wt.% oxides) $n = 6$	Standard deviation	Mean (wt.% oxides) $n = 6$	Standard deviation	Mean (wt.% oxides) $n = 9$	Standard deviation
Na_2O	0.04	0.04	0.03	0.02	0.03	0.03
MgO	34.57	2.67	34.72	1.03	37.28	2.11
Al_2O_3	0.14	0.11	2.82	1.09	0.09	0.05
SiO_2	42.26	2.26	38.15	0.85	42.58	0.65
K_2O	0.10	0.14	0.03	0.03	0.07	0.08
CaO	0.11	0.06	0.03	0.01	0.08	0.05
TiO_2	0.03	0.04	0.04	0.03	0.01	0.02
Cr_2O_3	0.01	0.02	0.77	0.15	0.04	0.05
MnO	0.07	0.07	0.07	0.09	0.08	0.07
FeO*	4.08	2.07	3.53	0.13	3.00	1.65
NiO	0.48	0.20	0.22	0.07	0.25	0.18
Total	81.88	2.05	80.40	1.05	83.51	1.09

* Total iron expressed as FeO (as Fe measured on rock-forming minerals).

https://doi.org/10.1346/CCMN.2006.0540111 Published online by Cambridge University Press

Table 2. EMPA (n analyses) of chlorites in the unweathered rock (wt.% oxides and corresponding structural formulae).

	Chlorites			
	Mean (wt.% oxides) n = 12	Standard deviation	Element	Structural formula**
Na_2O	0.02	0.02	Si	3.14
MgO	31.13	1.04	^{IV}Al	0.86
Al_2O_3	14.22	1.27	^{VI}Al	0.82
SiO_2	31.37	1.02	Fe^{2+}	0.28
K_2O	0.05	0.04	Ti	0.01
CaO	0.06	0.04	Mn	0.00
TiO_2	0.07	0.05	Ni	0.01
Cr_2O_3	1.99	0.24	Cr	0.16
MnO	0.03	0.05	Mg	4.65
FeO*	3.34	0.33	Octahedral	5.92
NiO	0.18	0.12	occupancy	
Total	82.45	1.6647		

* Total iron expressed as FeO (as Fe measured on rock-forming minerals)
** Atoms on the basis of 14 O_2

from the serpentinization effects where chromite can be replaced wholly or partially by secondary magnetite (Springer, 1974).

Weathering sequences

Weathered serpentine minerals. The first stages of rock weathering are observed at the saprock level and affect only the serpentine minerals with various microscopic features depending on the serpentine habits: (1) mesh serpentine textures and veins acquire a yellowish color without morphological change under plane-polarized light whereas; (2) thin-bladed texture, associated with a small amount of chlorite, retains its rock-forming habit. These initial weathering stages are characterized by the preservation of the mineral outlines although cores of brown-colored serpentines are replaced by clay minerals.

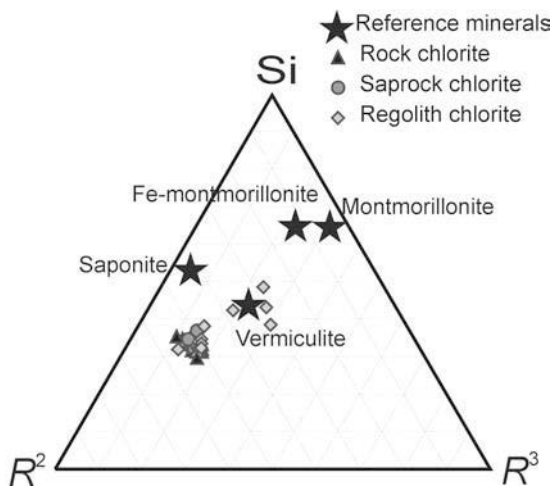

Figure 3. Rock and weathering products of chlorite analyses plotted in a Si–R^2–R^3 ternary projection. $R^2 = Mg^{2+} + Fe^{2+}$; $R^3 = Al^{3+} + Fe^{3+}$.

The results of EMPA of serpentine alteration products are given in Table 4a. Three types of smectites (Table 4b) with various chemical compositions were identified: (1) a poorly aluminous saponite from thin-bladed textures; (2) a Fe-rich montmorillonite ('MH') from mesh and hourglass textures, and (3) another Fe-rich montmorillonite ('V') from veins.

Except for saponite, the clays are very Fe-rich. The terminology for nontronite (tetrahedral charged smectite) and Fe montmorillonite (octahedral charged smectite) is based only on charge location.

In more advanced weathering stages in the regolith level, serpentine mineral outlines begin to disappear while dissolution cavities occur close to microcracks. The cavities are filled with clayey plasma and newly formed oxides and hydroxides. Petrographic observations show the existence of a clay mineral not associated with a rock-forming mineral and which is coating the previous weathered minerals. The EMPA results of the clay mineral reveal a nontronite composition.

Chemical compositions of secondary products from serpentine were plotted in a Si–R^2–R^3 ternary projection in order to illustrate the weathering path of serpentine minerals and the specific clay minerals formed from various serpentine textures (Figure 4). The early weathering stages are characterized by: (1) a local preservation of the Mg content with saponite formation from more resistant thin-bladed serpentine weathering; and (2) a Mg decrease and a relative enrichment of Si due to the intense weathering of mesh and vein serpentines (Caillaud *et al*., 2004), producing dioctahedral smectites rich in the less mobile elements, *i.e.* Fe and Al.

The regolith level is characterized by an important increase of Fe and Al concentrations. The chemical discrepancy between saprock and regolith clays (ferruginous clays in the saprock compared to more aluminous

https://doi.org/10.1346/CCMN.2006.0540111 Published online by Cambridge University Press

Table 3. EMPA (*n* analyses) of magnetites and chromites in the unweathered rock (wt.% oxides).

	Magnetites		Chromites	
	Mean (wt.% oxides) $n = 10$	Standard deviation	Mean (wt.% oxides) $n = 6$	Standard deviation
MgO	2.28	1.77	3.10	1.91
Al_2O_3	0.49	0.61	1.22	0.29
SiO_2	2.26	0.98	1.28	2.58
TiO_2	0.03	0.02	1.11	0.18
Cr_2O_3	0.43	0.46	40.50	4.17
MnO	0.07	0.05	0.50	0.15
FeO*	83.45	5.76	44.82	2.15
NiO	0.17	0.25	0.26	0.09
Total	89.21	4.08	92.87	3.09

* Total iron expressed as FeO (as Fe measured on rock-forming minerals).

clays in the regolith) is related to the formation of Fe oxides in the regolith (Caillaud *et al*., 2004) which have trapped most of the Fe, creating an Fe-depleted environment leading to crystallization of aluminous clay minerals.

Weathering products of chlorites. The chlorite minerals observed in thin-sections in the saprock level retain their rock-forming habit although some crystals exhibit exfoliated cleavage terminations. This exfoliation increases in the regolith level allowing the growth of yellowish clay minerals inside chlorite cleavages (Figure 5). The most noticeable changes in chlorite habit appear at the top of the regolith level where chlorite becomes intensely exfoliated with yellowish-brown color under plane-polarized light and blue to yellow bright tints under crossed nicols.

The XRD patterns of the weathering products of chlorites have the characteristics of a swelling clay mineral with a d_{001} value of 14.20 Å in the air-dried state, and of 17.20 Å after ethylene glycol solvation (Figure 6a). Intercalation of alkylammonium ions (nC = 12) gives a d_{001} value of 22.80 Å indicating a mean layer charge of 0.69 per half unit-cell (Figure 6b). This high value corresponds to a high-charge smectite.

The EMPA analyses of chlorite crystals in thin-sections in the saprock and regolith levels were used to calculate the mean structural formulae on the basis of 14 oxygen atoms. These structural formulae plotted in a Si-R^2-R^3 ternary diagram (Figure 3) show the homogeneous composition of the chlorite in the saprock level in comparison with the rock, in agreement with the conservation of the initial habit. Some chlorites analyzed in the regolith are slightly enriched in Si and Fe, indicating the beginning of chlorite weathering.

Other analyses in the regolith level reveal the complete transformation of chlorite in vermiculite (Figure 3), in agreement with petrographic observations and XRD results. Indeed, the fine focused electron microprobe spot (1 µm diameter) on cleavages of

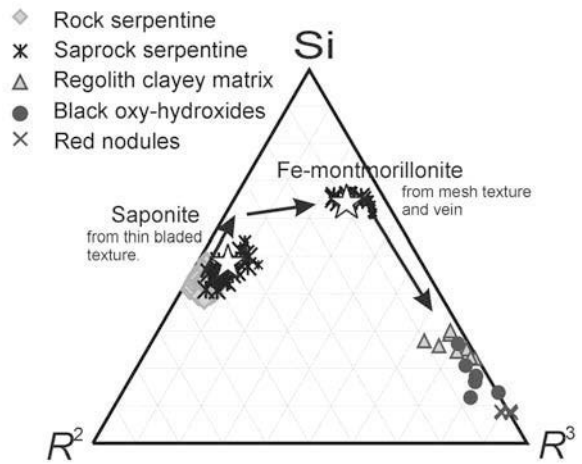

Figure 4. Synthesis of specific clay minerals formed from various serpentine minerals – representation of serpentine microsystems in a Si–R^2–R^3 ternary projection. R^2 = Mg + Fe^{2+}; R^3 = Al^{3+}+Fe^{3+}.

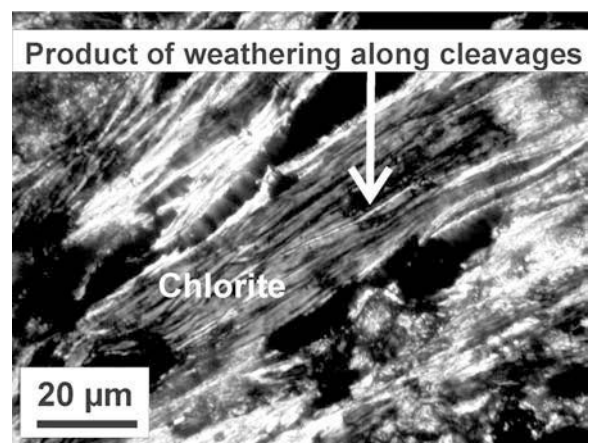

Figure 5. Optical micrograph, under crossed nicols, of weathering products of chlorite along cleavages.

https://doi.org/10.1346/CCMN.2006.0540111 Published online by Cambridge University Press

Table 4. (a) EMPA (*n* analyses) of secondary products from serpentine weathering (wt.% oxides).

	Fe-rich montmorillonite (MH) from mesh and hourglass textures		Saponite from thin blades		Fe-montmorillonite (V) from serpentine veins	
	Mean $n = 5$	Standard deviation	Mean $n = 6$	Standard deviation	Mean $n = 5$	Standard deviation
Na_2O	0.05	0.06	0.02	0.02	0.05	0.02
MgO	4.96	1.39	21.61	3.28	3.49	0.59
Al_2O_3	1.2	0.83	0.67	0.25	0.73	0.09
SiO_2	43.28	4.37	39.28	3.25	45.08	4.5
K_2O	0.08	0.1	0.03	0.02	0.04	0.02
CaO	0.11	0.2	0.03	0.03	0.03	0.04
TiO_2	0.08	0.06	0.01	0.01	0.05	0.04
Fe_2O_3*	20.23	2.81	11.90	2.28	22.34	2.65
NiO	1.02	0.16	0.63	0.11	0.78	0.07
Total	70.96	1.52	73.98	1.46	71.26	1.60

* Total iron expressed as Fe_2O_3 (as Fe measured on oxidized products)

(b) Structural formulae of secondary products from serpentine weathering (from *n* analyses).

Fe-rich montmorillonite (MH) from mesh and hourglass textures			Saponite from thin blades			Fe-montmorillonite (V) from serpentine veins	
	Mean $n = 5$	Standard deviation		Mean $n = 6$	Standard deviation	Mean $n = 5$	Standard deviation
Si	3.99	0.07	Si	3.44	0.10	Si 3.97	0.02
^{IV}Charge	0.02	0.07	^{IV}Charge	0.56	0.10	^{IV}Charge 0.03	0.02
^{IV}Al	0.02	0.07	^{IV}Al	0.07	0.02	^{IV}Al 0.03	0.02
^{IV}Fe	0.00	0.00	^{IV}Fe	0.49	0.12	^{IV}Fe 0.00	0.00
^{VI}Al	0.12	0.08	^{VI}Al	0.00	0.00	^{VI}Al 0.05	0.02
^{VI}Fe*	1.40	0.11	^{VI}Fe*	0.29	0.24	^{VI}Fe* 1.64	0.05
^{VI}Mg†	0.53	0.18	^{VI}Mg†	2.58	0.38	^{VI}Mg† 0.31	0.06
Octahedral occupancy	2.06	0.08	Octahedral occupancy	2.87	0.14	Octahedral occupancy 2.00	0.02
^{VI}Charge	0.35	0.07	^{VI}Charge‡	−0.06	0.04	^{VI}Charge 0.31	0.03
Total charge	0.37	0.05	Total charge	0.50	0.08	Total charge 0.33	0.01
Interlayer	0.34	0.04	Interlayer	0.50	0.07	Interlayer 0.32	0.00

* Total iron expressed as Fe_2O_3 (as Fe measured on oxidized products)
† ^{VI}Mg = (Mg total − Mg exchangeable) with Mg exchangeable calculated = 0.15
‡ Overcharged octahedral sheet

weathering products of chlorites allowed analysis of their secondary clay minerals (Table 5a); chlorite-derived clays show trioctahedral vermiculite and dioctahedral high-charged smectite compositions (Table 5b). The differences between the two clay minerals are the Si, Mg and Fe and contents. The structural formulae of trioctahedral vermiculite show a larger amount of Al when compared to dioctahedral high-charge smectite (0.82 *vs*. 0.58 atom) and Mg (2.33 *vs*. 1.21 atom), and lower Fe content (0.811 *vs*. 1.01 atom). Both are characterized by a high tetrahedral charge.

The SEM observations, in secondary electron mode, of isolated chlorite pasted on a glass section show the crystals to have a platy morphology which can reach >300 μm size (Figure 7). Its surface appears smooth and homogeneous, but, at higher magnification, smaller platy particles are observed coating the chlorite surface, especially along cleavage planes. In backscattered electron mode, these surfaces show chemical variations between the small particles and the rock-forming chlorite. Actually, the coatings appear brighter than the chlorites (uniform gray) indicating a composition richer in heavy elements. Qualitative spectra acquired in secondary electron mode indicate that small particles are richer than chlorites in Fe and Si whereas they have lower Al and Mg contents in their structure. The coating particles observed at higher magnification in secondary electron mode reveal irregular outlines and are composed of packed platelets which parallel the chlorite surface.

Chemical compositions of chlorite alteration products were plotted in a Si$-R^2-R^3$ ternary projection in order

https://doi.org/10.1346/CCMN.2006.0540111 Published online by Cambridge University Press

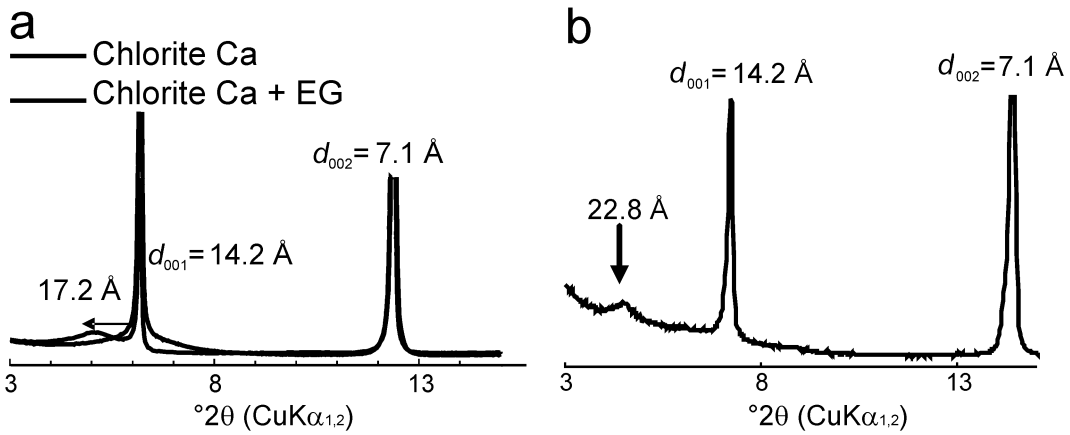

Figure 6. (a) XRD oriented patterns of Ca-saturated chlorite; air-dried (Chlorite Ca) and ethylene glycol-solvated (Chlorite Ca + EG). Swelling clay mineral with 14.20 Å d_{001} spacing in the air-dried state, and 17.20 Å d_{001} spacing after ethylene glycol solvation. (b) XRD oriented pattern of alkylammonium-saturated chlorite (according to the method of Olis *et al*., 1990): empirical method to determine the mean layer charge from d_{001} values obtained after expansion of the clay minerals with single, long-chain alkylammonium ions (nC = 12). Intercalation of alkylammonium ions (nC = 12) gives a d_{001} spacing of 22.80 Å indicating a mean layer charge of 0.69 per half unit-cell.

to show the specific clay minerals formed from chlorite (Figure 8).

Weathered magnetite and chromite. Microscopic observation under reflected or transmitted light of the weathered magnetite and chromite from the saprock level shows a slight decrease in their reflectance along edges, together with the development of darkish halos which diffuse in the cracks crosscutting the crystals. Some specific Fe accumulation habits (Figure 9) are observed in the regolith levels: (1) red nodules, (2) dark brown segregations mixed with clayey matrix and (3) black oxyhydroxides often associated with chlorites.

The XRD patterns of isolated magnetic particles (Figure 10) indicate that newly formed Fe oxides appear: maghemite (2.53, 2.97, 1.61, 2.10 Å), goethite (4.18, 2.69, 2.45 Å) and to a lesser extent, hematite (2.70, 3.68, 2.52, 1.70, 1.83 Å). A sharp increase in goethite contents in the saprock, between 100 and 120 cm, is locally observed. The EMPA results of these oxyhydroxides are given in Table 6.

Fissural clays. The fissures observed in thin-sections from the saprock and regolith levels are often rimmed with clayey deposits. The EMPA results of these deposits indicate some Mg- and Fe-rich clay minerals in the different weathered levels with a small Si content thus inducing an important tetrahedral charge deficit. Because the total charge distribution in the structure and fraction of Mg as the interlayer cation is not known, we cannot identify the clay minerals accurately (vermiculite or smectite).

DISCUSSION

Serpentine habits and crystal structures

The petrographic study allows us to identify two serpentine textures, *i.e.* (1) pseudomorphic textures with mesh, hourglass and thin-bladed habits, associated with serpentine fiber rims, and (2) serpentine veins crosscutting the whole rock. Pseudomorphic textures have been described extensively in the literature (Whittaker and Zussman, 1956; Green, 1961; Hochstetter, 1965; Coleman, 1966; Page, 1967, 1968; Aumento, 1970; Boudier, 1971; Coleman and Keith, 1971; Wicks and Whittaker, 1977) as mesh, hourglass and bastite assemblages (bastites are most commonly pseudomorphic textures after pyroxene and/or amphibole) composed mainly of various combinations of lizardite, chrysotile and brucite.

In this study, the XRD pattern on the unweathered rock indicates only the presence of lizardite (1T-2T-3R) and chrysotile $2Or_{c1}$ as serpentine minerals. Lizardite is found in pseudomorphic textures, *i.e.* mesh, hourglass and thin-bladed (bastite) textures, whereas serpentine veins are composed of orthochrysotile. This mineralogy is similar to that described by Wicks and Whittaker (1977). Besides, the chemical variations between these textures are in good agreement with those measured for lizardite and chrysotile by Whittaker and Wicks (1970) and for lizardite bastite by Dungan (1974).

The absence of antigorite minerals in the studied serpentinite suggests serpentinization conditions. From the literature, antigorite is said to form at higher temperatures than lizardite and chrysotile. Indeed, the lizardite-chrysotile serpentinites probably form at temperatures of not more than 200ºC (Moody, 1976). Besides, antigorite-rich serpentinite is reported to form in the presence of non-meteoritic waters (Wenner and Taylor, 1974). Those authors stated that lizardite-chrysotile serpentinization is probably caused by waters of meteoritic-hydrothermal origin or by waters in sedimentary formation which contain a major meteoritic water component.

https://doi.org/10.1346/CCMN.2006.0540111 Published online by Cambridge University Press

Table 5. (a) EMPA (*n* analyses) of secondary products from chlorite weathering (wt.% oxides).

	Vermiculite		High-charged smectite	
	Mean $n = 12$	Standard deviation	Mean $n = 10$	Standard deviation
Na_2O	0.01	0.02	0.03	0.03
MgO	23.30	1.42	13.65	2.62
Al_2O_3	9.20	0.86	6.62	1.71
SiO_2	37.15	2.12	47.08	3.21
K_2O	0.01	0.01	0.04	0.06
CaO	0.03	0.03	0.03	0.02
TiO_2	0.13	0.08	0.11	0.07
Fe_2O_3*	14.13	3.04	18.07	3.13
Cr_2O_3	2.92	2.58	1.23	0.40
NiO	0.68	0.26	0.61	0.15
Total	75.56	1.17	78.73	1.37

* Total iron expressed as Fe_2O_3 (as Fe measured on oxidized products)

(b) Structural formulae per half unit-cell of secondary products from chlorite weathering. Atoms on the basis of 11 O_2.

	Vermiculite			High-charged smectite	
	Mean $n = 12$	Standard deviation		Mean $n = 10$	Standard deviation
Si	2.816	0.108	Si	3.488	0.177
^{IV}Charge	1.184	0.108	^{IV}Charge	0.512	0.177
^{IV}Al	0.821	0.060	^{IV}Al	0.502	0.174
^{IV}Fe	0.362	0.151	^{IV}Fe	0.010	0.029
^{VI}Al	0.000	0.000	^{VI}Al	0.077	0.075
^{VI}Fe*	0.449	0.113	^{VI}Fe*	0.997	0.152
^{VI}Mg†	2.334	0.131	^{VI}Mg†	1.214	0.316
^{VI}Cr	0.173	0.149	^{VI}Cr	0.072	0.025
Octahedral occupancy	2.956	0.043	Octahedral occupancy	2.360	0.157
^{VI}Charge‡	−0.534	0.096	^{VI}Charge	0.133	0.172
Total charge	0.650	0.019	Total charge	0.645	0.024
Interlayer	0.608	0.004	Interlayer	0.612	0.008

* Total iron expressed as Fe_2O_3 (as Fe measured on oxidized products).
† ^{VI}Mg = (Mg total−Mg exchangeable) with Mg exchangeable calculated = 0.3.
‡ Overcharged octahedral sheet.

Table 6. EMPA (*n* analyses) of oxy-hydroxides in the weathered zones (wt.% oxides).

	Red nodules		Black oxyhydroxides		Clayey matrix	
	Mean $n = 8$	Standard deviation	Mean $n = 8$	Standard deviation	Mean $n = 10$	Standard deviation
MgO	0.09	0.04	0.68	0.38	2.78	4.01
Al_2O_3	1.53	0.43	1.47	1.10	4.33	1.62
SiO_2	3.13	0.38	4.65	2.73	11.44	7.09
TiO_2	0.06	0.05	0.05	0.07	0.06	0.04
Cr_2O_3	1.29	0.70	0.07	0.10	0.44	0.29
MnO	0.10	0.08	19.00	8.82	0.07	0.10
Fe_2O_3*	72.58	0.90	27.27	9.61	55.40	10.68
NiO	0.28	0.06	6.53	1.67	0.55	0.27
Total	77.96	0.91	53.29	5.57	74.50	4.92

* Total iron expressed as Fe_2O_3 (as Fe measured on oxidized products)

https://doi.org/10.1346/CCMN.2006.0540111 Published online by Cambridge University Press

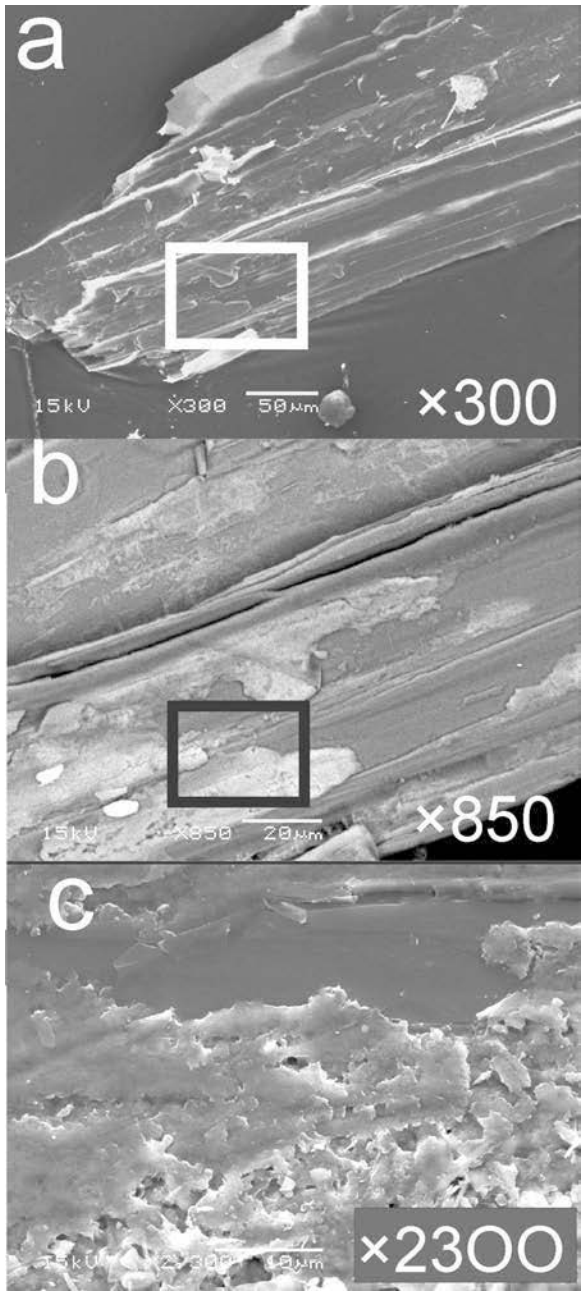

Figure 7. Scanning electron micrographs of chlorites under secondary (SEI) and backscattered electron modes (BEIC): (a) chlorite crystal; (b) coating vermiculite (BEIC); (c) enlargement of vermiculite platelet (SEI).

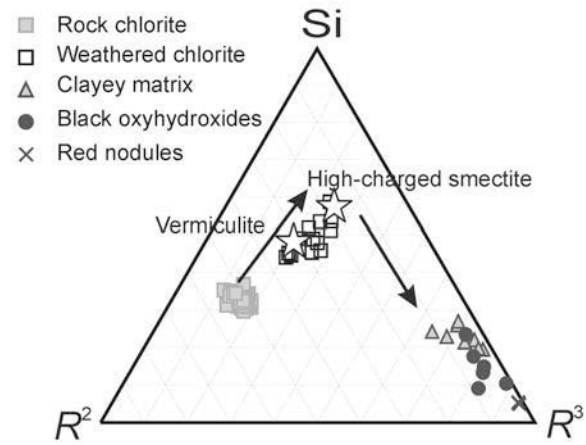

Figure 8. Synthesis of specific clay minerals formed from chlorite minerals – representation of chlorite microsystems in a $Si-R^2-R^3$ ternary projection. $R^2 = Mg + Fe^{2+}$; $R^3 = Al^{3+}+Fe^{3+}$.

Weathering sequences of rock-forming minerals

In the early weathering stage, the rock structure is preserved. The petrographic study has shown different textures for serpentine minerals described previously: (1) lizardite mesh and hourglass textures, (2) lizardite thin blades (bastites) and (3) chrysotile veins. Electron microprobe analyses indicate that specific clay minerals formed in these particular weathering microsites of parental serpentine minerals (Figure 4). (1) A dioctahedral Fe-rich smectite (Fe montmorillonite, MH) is formed from mesh and hourglass-texture weathering. (2) A trioctahedral Mg smectite (saponite) is formed from weathering of thin-bladed serpentine. (3) A dioctahedral Fe-rich smectite (Fe montmorillonite, V) is formed from chrysotile vein weathering. Some nontronite is also formed from either non-pseudomorphic textures or from opening previous textures.

The structural formulae (Table 4b) of Fe montmorillonite MH show larger amounts of Al in octahedral sites when compared to montmorillonite V (0.12 *vs*. 0.05 atoms), Mg (0.53 *vs*. 0.31 atoms) and smaller Fe content (1.40 *vs*.1.64 atoms).

The EMPA results of the two Fe montmorillonites have been compared with those of their parent minerals (Table 7). As chrysotile veins are poorer in Al (0.09 *vs*. 0.14 wt.% oxides) and contain more Mg (37.28 *vs*. 34.57 wt.% oxides) than mesh serpentines, they lose Mg more easily (depletion factor: 11 *vs*. 7). Besides, Al is considered to be the immobile element during the weathering processes (Caillaud *et al.*, 2004). Thus, the lack of Al in veins is compensated by Fe (concentration factor: 7.5 *vs*. 5) and explains why montmorillonite V is richer in Fe than montmorillonite MH. As petrographic observations show similar weathering rates for mesh and vein serpentines, *i.e* the two serpentine structures are identically sensitive to the Mg leaching in the first stages of rock weathering, the compositional variation between smectites seems to be directly controlled by chemistry of the parent minerals (*e.g*. amphibole: Banfield and Barker, 1994).

The saponite occurring in the thin blades has a particular structural formula (Table 4b) with a very small amount of tetrahedral Al (0.07 atom) and a large amount of tetrahedral Fe (0.49 atoms), which is very atypical of a saponite. Besides, this clay mineral results from the weathering of thin blades (lizardite, bastite)

https://doi.org/10.1346/CCMN.2006.0540111 Published online by Cambridge University Press

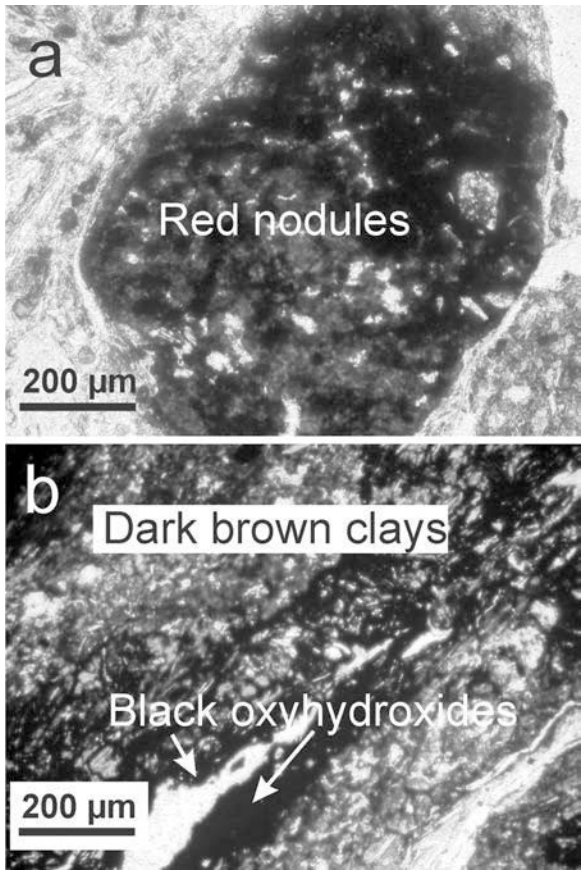

Figure 9. Iron features in a regolith zone derived from oxide weathering: (a) red nodules; (b) black oxyhydroxides surrounded by dark brown segregations mixed with a clayey matrix.

which have the larger Al content among the serpentines. However, petrographic study shows that small chlorites are interlocking into the thin blades probably causing an overestimation of Al in the bastite lizardite composition. This chlorite contamination of lizardite bastite is much more evident from its high Cr content which is more typical of the Cr-bearing chlorites. Thus, pure lizardite bastite should probably contain very little Al, thus producing Al-poor saponite.

Moreover, thin lizardite bastite has a smaller Si content than other serpentines. This could explain the highly tetrahedral-charged saponites resulting from their weathering. Contrary to the other secondary minerals observed in serpentine textures, the saponite is the only Mg-bearing phase. The Mg is the major exchangeable cation during these weathering processes (Caillaud *et al.*, 2004). As petrographic observations indicate that thin blades are more resistant to weathering than mesh, hourglass textures and chrysotile veins, they are, thus, a Mg source for the saponite formation.

Specific clay minerals formed from chlorite minerals especially in the regolith zone (Figure 8) are (1) a trioctahedral vermiculite and (2) a dioctahedral high-charged smectite; the latter is enriched in Fe and has a lower Mg content. As a consequence, the dioctahedral high-charged smectite seems to result from a more advanced weathering stage than the trioctahedral vermiculite. Besides, the chemical results show that vermiculite is richer in Al than dioctahedral high-charged smectite. The weathering of chlorite, which is the only Al bearing-phase, liberates increasing amounts of Al in the upper horizons which is partially trapped in Fe-rich

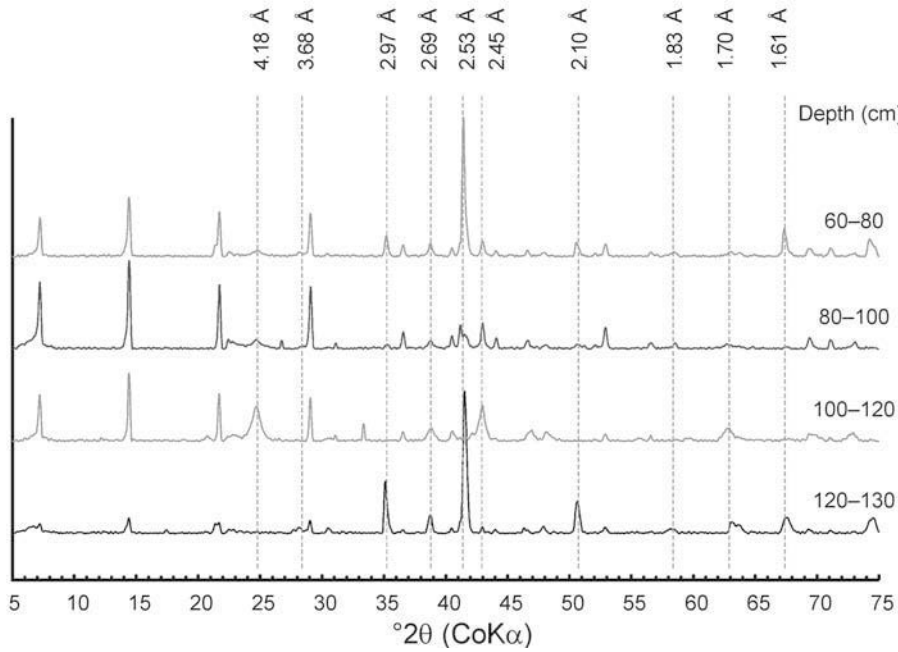

Figure 10. XRD powder pattern of the magnetic fraction. Magnetite/maghemite (2.53, 2.97, 1.61, 2.10 Å), goethite (4.18, 2.69, 2.45 Å), hematite (2.70, 3.68, 2.52, 1.70, 1.83 Å). Non-annotated peaks correspond to the clinochlore reflections.

https://doi.org/10.1346/CCMN.2006.0540111 Published online by Cambridge University Press

Table 7. EMPA (*n* analyses) of the secondary products, Fe-montmorillonite, MH and V, from mesh serpentine and vein weathering, respectively (wt.% oxides).

Element	Mesh serpentine Mean (wt.% oxides) $n = 6$	Fe-montmorillonite MH Mean (wt.% oxides) $n = 5$	Standard deviation	Serpentine vein Mean (wt.% oxides) $n = 9$	Fe-montmorillonite V Mean (wt.% oxides) $n = 5$	Standard deviation
Na_2O	0.04	0.05	0.06	0.03	0.05	0.02
MgO	34.57	4.96	1.39	37.28	3.49	0.59
Al_2O_3	0.14	1.2	0.83	0.09	0.73	0.09
SiO_2	42.26	43.28	4.37	42.58	45.08	4.5
K_2O	0.10	0.08	0.1	0.07	0.04	0.02
CaO	0.11	0.11	0.2	0.08	0.03	0.04
TiO_2	0.03	0.08	0.06	0.01	0.05	0.04
FeO* Fe_2O_3**	4.08	20.23	2.81	3.00	22.34	2.65
NiO	0.48	1.02	0.16	0.25	0.78	0.07

* Total iron expressed as FeO for unweathered serpentines (as Fe measured on rock-forming minerals).
** Total iron expressed as Fe_2O_3 for weathered products (as Fe measured on oxidized products).

smectites (Caillaud *et al.*, 2004). This suggests that high-charged smectite is issued from a more advanced weathering rate.

With the exception of magnetite and chromite, all of the oxyhydroxides, *i.e.* maghemite, goethite and hematite, have been identified as products of pedogenesis. From the early weathering zone, the magnetite minerals are transformed partially into crystallized phases as maghemite (Figure 10). Indeed, maghemite prevailed in soils formed from basic igneous rock, mostly derived from oxidation of magnetite (Schwertmann and Taylor, 1977). Figure 10 shows that maghemite and hematite prevail at the 120−130 cm and 60−80 cm levels whereas goethite occurs mainly in the 100−120 and 80−100 cm horizons. The distribution of oxyhydroxides in the profile may result from the moisture conditions. Indeed, the abundance of maghemite which is known to occur in concretions frequently in association with hematite (Schwertmann and Taylor, 1977), may be related to drier conditions at these levels. Goethite is the most frequently found form of Fe oxide in soils, occurring in almost all soil types and climatic areas, and is the most stable under most soil conditions (Schwertmann and Taylor, 1977).

Relationship between weathering sequences at the microsite scale and bulk clay mineralogy

In the upper regolith, the initial rock structure is destroyed. Mineral outlines disappear and clay minerals and oxides are reorganized into a new structure. Some important clayey accumulation appears in an orange 'plasma' habit including new oxyhydroxides which create new chemical conditions. Increasing weathering opens the system. The element redistribution is thus governed by the modification of the element-bearing phases and is influenced by the weathering solution. Except for the saponite mineral and some fissural microsites, the weathering products in rock are strongly leached in Mg and enriched in Fe. This tendency is in agreement with (1) the formation of nontronite phases from more 'open' textures in which mineral outlines begin to disappear and (2) the bulk clay chemistry which presents an Fe-rich smectite composition (Caillaud *et al.*, 2004). The important development of the mesh and hourglass textures in comparison to the thin blades tend to increase the quantity of Fe montmorillonite which forms in the weathered levels. In the same manner, the small chlorite contents in the rock and their poor weathering susceptibility induces the formation of only a little vermiculite which is not identified in the bulk clay.

The usual mineral transformations proceed through two main mechanisms: (1) solution-mediated solid-state transformation; and (2) dissolution/crystallization transformation. Some tentative criteria to distinguish the two main intermineral transformation mechanisms are based on the crystal habit and chemical inheritance (Baronnet, 1997). In this study, the mineral transformations are characterized by a strong modification of the rock-forming mineral habit and by a new secondary chemical composition. In spite of the lack of other criteria (topotaxy, polytype inheritance, chemical and structural homogeneity, defect inheritance), the main mechanism occurring during weathering processes is a dissolution/crystallization transformation.

CONCLUSIONS

These results indicate that the mineralogical complexity characterizing the weathering products found in the serpentinite arises from the heterogeneity of the serpentine textures in the rock, the occurrence of additional rock-forming minerals (chlorite and oxides) and the diversity of their corresponding weathering

https://doi.org/10.1346/CCMN.2006.0540111 Published online by Cambridge University Press

microsites in the profile. During clay formation, the microstructure of clay rock-soil systems changes: (1) the element leaching or fixation depends on local rock chemical properties in the saprock (microsystems); whereas (2) in the upper stage, a new more porous microstructure changes the chemical conditions which are now controlled by the percolating solutions. The problem of separating the rock-forming minerals has required the *in situ* measurement of the weathering product chemistry in order to identify the clay minerals.

REFERENCES

Alexander, E.B., Adamson, C., Zinke, P.J. and Graham, R.C. (1989) Soils and conifer productivity on serpentinized peridotite of the Trinity ophiolite, California. *Soil Sciences*, **148**, 412–423.

Aumento, F. (1970) Serpentine mineralogy of ultrabasic intrusions in Canada and the Mid-Atlantic Ridge. *Geological Survey of Canada Paper*, **69-53**, 51 pp.

Bailey, S.W. (1969) Polytypism of trioctahedral 1:1 layer silicates. *Clays and Clay Minerals*, **17**, 355–371.

Bailey, S.W. (1980) Structures of layer silicates. Pp. 1–23 in: *Crystal Structures of Clay Minerals and their X-ray Identification* (G.W. Brindley and G. Brown, editors). Monograph **5**, Mineralogical Society, London.

Banfield, J.F. and Barker, W.W. (1994) Direct observation of reactant-product interfaces formed in natural weathering of exsolved defective amphibole to smectite: evidence of episodic, isovolumetric reactions involving structural inheritance. *Geochimica et Cosmochimica Acta*, **58**, 1419–1429.

Barnes, I. and O'Neil, J.R. (1969) The relationship between fluids in some fresh Alpine-type ultramafics and possible modern serpentinization, Western U.S. *Bulletin of the Geological Society of America*, **80**, 1947–1960.

Barnes, I., Rapp, J.B. and O'Neil, J.R. (1972) Metamorphic assemblages and the direction of flow of metamorphic fluids in four instances of serpentinization. *Contributions to Mineralogy and Petrology*, **35**, 263–276.

Baronnet, A. (1997) Silicate microstructures at the subatomique scale. *Compte rendu de l'Académie des Sciences de Paris*, **324**, série IIa, 157–172.

Bates, T.F. (1951) Morphology of layer lattice silicates. *Journal of the Scientific Laboratories of Denison University*, **42**, 83–91.

Bates, T.F. (1959) Morphology and crystal chemistry of 1:1 layer lattice silicates. *American Mineralogist*, **44**, 78–114.

Berre, A., Ducloux, J. and Dupuis, J. (1974) Pédogénèse sur roches ultrabasiques en climat tempéré humide : les sols sur serpentinites du Limousin occidental. *Science du sol. Bulletin de l'AFES*, **3**, 135–146.

Bonifacio, E., Zanini, E., Boero, V. and Franchini-Angela, M. (1996) Pedogenesis in a soil catena on serpentinite in northwestern Italy. *Geoderma*, **75**, 33–51.

Boudier, F. (1971) Minéraux serpentineux extraits de péridotites serpentinisées des Alpes Occidentales. *Contributions to Mineralogy and Petrology*, **33**, 331–345.

Bulmer, C.E and Lavkulich, L.M. (1994) Pedogenic and geochemical processes of ultramafic soils along a climatic gradient in southwestern British Columbia. *Canadian Journal of Soil Science*, **74**, 165–177.

Caillaud, J., Proust, D., Righi, D. and Martin, F. (2004) Iron-rich clays in a weathering profile developed from serpentinite. *Clays and Clay Minerals*, **52**, 779–791.

Chernosky, J.V. (1973) The stability of chrysotile, $Mg_3Si_2O_5(OH)_4$, and the free energy of formation of talc, $Mg_3Si_4O_{10}(OH)_2$. *Geological Society of America Annual Meeting, Program and Abstracts.*

Coleman, R.G. (1966) New Zealand serpentinites and associated metasomatic rocks. *New Zealand Geological Survey Bulletin N.S.*, **76**.

Coleman, R.G. (1971) Petrologic and geophysical nature of serpentinites. *Bulletin of the Geological Society of America*, **82**, 897–918.

Coleman, R.G. and Keith, T.E. (1971) A chemical study of serpentinization – Burro Mountain, California. *Journal of Petrology*, **12**, 311–328.

Coombe, D.E., Frost, L.C., Le Bas, M. and Watters, W. (1956) The nature of the soils over the Cornish serpentine. *Journal of Ecology*, 605–615.

Ducloux, J., Meunier, A. and Velde, B. (1976) Smectite, chlorite, and a regular interlayered chlorite-vermiculite in soils developed on a small serpentinite body, Massif Central, France. *Clay Minerals*, **11**, 121–135.

Dungan, M.A. (1974) The origin, emplacement and metamorphism of the sultan Mafic-Ultramafic Complex, Northern Cascades, Snohomish County, Washington. PhD dissertation, University of Washington, Seattle, Washington.

Fontanaud, A. (1982) Les faciès d'altération supergène des roches ultrabasiques. Etude de deux massifs de lherzolite (Pyrénées, France). Thèse 3ème cycle, Université de Poitiers, 103 pp.

Graham, R.C., Diallo, M.M. and Lund, L.J. (1990) Soils and mineral weathering on phyllite colluvium and serpentinite in northwestern California. *Soil Science Society of America Journal*, **54**, 1682–1690.

Green, D.H. (1961) Ultramafic breccias from the Musa Valley, eastern Papua. *Geological Magazine*, **98**, 1–26.

Hochella, M.F. and Banfield, J.F. (1996) Chemical weathering of silicates in nature: a microscopic perspective with theoretical considerations. Pp. 353–406 in: *Chemical Weathering Rates in Silicate Minerals* (A.F. White and S.L. Brantley, editors). Reviews in Mineralogy, **31**, Mineralogical Society of America, Washington, D.C.

Hochstetter, R. (1965) Zur Kenntnist der Serpentinmineralien. PhD thesis, Universität des Saarlandes, Germany.

Hostetler, P.B., Coleman, R.G., Mumpton, F.A. and Evans, B.W. (1966) Brucite in Alpine serpentinites. *American Mineralogist*, **51**, 75–98.

Ildefonse, P. (1978) Mécanismes de l'altération d'une roche gabbroïque du Massif du Pallet (Loire-Atlantique). Thèse 3ème cycle, Université de Poitiers, 142 pp.

Istok, J.D. and Harward, M.E. (1982) Influence of soil moisture on smectite formation in soils derived from serpentinite. *Soil Science Society of America Journal*, **46**, 1106–1108.

Johannes, W. (1968) Experimental investigation of the reaction forsterite + water = serpentine + brucite. *Contributions to Mineralogy and Petrotrology*, **19**, 309–315.

Johannes, W. and Metz, P. (1968) Experimentelle Bestimmung von Gleichgewilchlsbeziehungen im System $MgO–CO_2–H_2O$. *Neues Jahrbuch für Mineralogie Monatshefte*, **16**, 15–26.

Lee, B.D., Graham, R.C., Laurent, T.E., Amrhein, C. and Creasy, R.M. (2001) Spatial distributions of soil chemical conditions in a serpentinic wetland and surrounding landscape. *Soil Science Society of America Journal*, **65**, 1183–1196.

Lee, B.D., Sears, S.K., Graham, R.C., Amrhein, C. and Vali, H. (2003) Secondary mineral genesis from chlorite and serpentine in an ultramafic soil toposequence. *Soil Science Society of America Journal*, **67**, 1309–1317.

Meunier, A. (1977) Les mécanismes d'altération des granites et le rôle des microsystèmes. Etude des arènes du massif granitique de Parthenay (Deux-Sèvres). Thèse Sciences,

https://doi.org/10.1346/CCMN.2006.0540111 Published online by Cambridge University Press

Université de Poitiers, France, 248 pp.
Moody, J.B. (1974) Serpentinization of iron-bearing olivines: an experimental study. PhD dissertation, McGill University, Montreal, Canada.
Moody, J.B. (1976) An experimental study on the serpentinization of iron-bearing olivines. *The Canadian Mineralogist*, **14**, 462–478.
Olis, A.C., Malla, P.B. and Douglas, L.A. (1990) The rapid estimation of the layer charges of 2:1 expanding clays from a single alkylammonium ion expansion. *Clay Minerals*, **25**, 39–50.
Page, N.J. (1967) Serpentinization at Burro Mountain, California. *Contributions to Mineralogy and Petrology*, **14**, 321–342.
Page, N.J. (1968) Serpentinization in a sheared serpentinite lens, Tiburon, Peninsula, California. *US Geological Survey Professional Paper*, **600-B**, 21–28.
Proust, D. (1983) Mécanismes d'altération supergène des roches ultrabasiques. Etude des arènes d'orthoamphibolite du Limousin et de glaucophanite de l'île de Groix (Morbihan). Thèse Sciences, Université de Poitiers, France, 197 pp.
Rabenhorst, M.C., Foss, J.E. and Fanning, D.S. (1982) Genesis of Maryland soils formed from serpentinite. *Soil Science Society of America Journal*, **46**, 607–616.
Roy, D.M. and Roy, R. (1954) An experimental study of the formation and properties of synthetic serpentines and related layer silicate minerals. *American Mineralogist*, **39**, 959–975.
Schwertmann, U. and Taylor, R.M. (1977) Iron oxides. Pp. 145–176 in: *Minerals in Soil Environments* (J.B. Dixon and S.B. Weed, editors). Soil Science Society of America. Madison, Wisconsin, USA.
Shirozu, H. (1978) Chlorite minerals. Pp 243–264 in: *Clays and Clay Minerals of Japan* (T. Sudo and S. Shimoda, editors). Elsevier, Amsterdam.
Springer, R.K. (1974) Contact metamorphosed ultramafic rocks in the Western Sierra Nevada foothills, California. *Journal of Petrology*, **15**, 160–195.
Wenner, D.B. and Taylor, H.P. (1971) Temperatures of serpentinization of ultramafic rocks based on O^{18}/O^{16} fractionation between co-existing serpentine and magnetite. *Contributions to Mineralogy and Petrology*, **32**, 165–185.
Wenner, D.B. and Taylor, H.P. (1974) D/H and O^{18}/O^{16} studies of serpentinization of ultramafic rocks. *Geochimica et Cosmochimica Acta*, **38**, 1255–1286.
Whittaker, E.J.W. and Wicks, F.J. (1970) Chemical differences among the serpentine 'polymorphs': a discussion. *American Mineralogist*, **55**, 1025–1047.
Whittaker, E.J.W. and Zussman, J. (1956) The characterization of serpentine minerals by X-ray diffraction. *Mineralogical Magazine*, **31**, 107–126.
Wicks, F.J. (1969) X-ray and optical studies of serpentine minerals. PhD dissertation, Oxford University, Oxford, England.
Wicks, F.J. and Whittaker, E.J.W. (1975) A reappraisal of the structures of the serpentine minerals. *The Canadian Mineralogist*, **13**, 227–243.
Wicks, F.J. and Whittaker, E.J.W. (1977) Serpentine textures and serpentinization. *The Canadian Mineralogist*, **15**, 459–488.
Wildman, W.E., Jackson, M.L. and Whittig, L.D. (1968) Iron-rich montmorillonite formation in soils derived from serpentinite. *Soil Science Society of America Proceedings*, **32**, 787–794.

(*Received 3 March 2005; revised 11 July 2005; Ms. 1038*)